Large-scale synoptic drivers of co-occurring summertime ozone and $PM_{2.5}$ pollution in eastern China

Lian Zong[1], Yuanjian Yang[1,*], Meng Gao[2], Hong Wang[1], Peng Wang[3], Hongliang Zhang[4], Linlin Wang[5], Guicai Ning[6], Chao Liu[1], Yubin Li[1], Zhiqiu Gao[1,5]

1. School of Atmospheric Physics, Nanjing University of Information Science & Technology, Nanjing, China
2. Department of Geography, Hong Kong Baptist University, Hong Kong SAR, China
3. Policy Research Center for Environment and Economy, Ministry of Ecology and Environment of the People's Republic of China, Beijing, China
4. Department of environmental science and engineering, Fudan University, China
5. State Key Laboratory of Atmospheric Boundary Layer Physics and Atmospheric Chemistry (LAPC), Institute of Atmospheric Physics, Chinese Academy of Sciences, Beijing, China
6. Institute of Environment, Energy and Sustainability, The Chinese University of Hong Kong, Shatin, N.T., Hong Kong, China

* Correspondence to: Dr./Prof. Y. Yang (yyj1985@nuist.edu.cn)

Abstract

Surface ozone (O_3) pollution during summer (June-August) over eastern China has become more severe, resulting in a co-occurrence of surface O_3 and $PM_{2.5}$ (particulate matter with aerodynamic diameter ≤ 2.5 μm in the air) pollution recently. However, the mechanisms regarding how synoptic circulation pattern could influence this compound pollution remains unclear. This study here applied the T-mode principal component analysis (T-PCA) method is used to objectively classify the occurrence of four synoptic weather patterns (SWPs) over eastern China, based on the geopotential heights at 500 hPa during summer (2015-2018). Four SWPs of eastern China are closely related to the western Pacific subtropical high (WPSH), exhibiting, significant intraseasonal and interannual variations. Based on the ground-level air quality and meteorological observations, remarkable spatial and temporal disparities of surface O_3 and $PM_{2.5}$ pollution were also found under the impacts of the four SWPs. Particularly, there were two SWPs sensitive to compound pollution (Type 1 and Type 2). Type 1 is characterized by a stable WPSH ridge with axis at about 22°N and the rain belt located in the south of Yangtze River Delta (YRD). High temperature, moderate humidity and low precipitation occurred in the region from BTH to northern YRD (BTH – NYRD), resulting in a co-occurrence of O_3 and $PM_{2.5}$ pollution. Additionally, air pollutants can be transported by the prevailing southerly winds from southern plains and accumulated in the southern BTH, resulting in a worsen pollution. Type 2 exhibits a WPSH dominance (the ridge axis ~25°N) and rain belt (over the YRD) in a higher latitude compared with Type 1. High temperature, medium-high humidity and low precipitation over the BTH were the conducive factors related to the occurrence of the compound pollution events under Type 2. Furthermore, low boundary layer height (BLH) and high frequency of light-wind days (FLWD) could create favorable conditions for pollution maintenance. Overall, synoptic weather patterns have played an important role as driving factors of surface O_3-$PM_{2.5}$ compound pollution in a regional context. In addition to the impacts of local emissions, our results may provide further insights regarding how regional environmental changes due to co-occurrence of high $PM_{2.5}$ and high O_3 level may be driven by the effects of meteorological factors. Overall, our findings demonstrate the important role played by synoptic weather patterns in driving regional surface O_3-$PM_{2.5}$ compound pollution, in addition to the large quantities of emissions, and may also provide insights into the regional co-occurring high $PM_{2.5}$ and high O_3 level

via the effects of certain meteorological factors.

Keywords: Synoptic weather pattern, ozone, $PM_{2.5}$, compound pollution, western Pacific subtropical high (WPSH)

1. Introduction

In recent years, China has been experiencing serious air pollution problems due to the enormous emissions of polluting gases [e.g., sulfur dioxide, nitrogen dioxide (NO_2), etc.] and aerosol particulates [e.g., particulate matter with aerodynamic diameter ≤ 2.5 (10) μm in the air $PM_{2.5}$ (PM_{10}), etc.] associated with its rapid economic development, industrialization and urbanization, together with certain unfavorable meteorological conditions (Wang & Chen, 2016; Zhang et al., 2014; Zhang et al., 2016). Particularly, atmospheric compound pollution has become serious (Li et al., 2019; Saikawa et al., 2017; Zhang et al., 2019a), especially for the economically developed and densely populated eastern urban agglomerations of China, such as the Beijing–Tianjin–Hebei (BTH), Yangtze River Delta (YRD) and Pearl River Delta (PRD) regions (Cai et al., 2017; Du et al., 2019; Ji et al., 2018; Li et al., 2020), exerting a severe threat in terms of public health, economy and society (Chen et al., 2019; Cohen et al., 2017; Day et al., 2017; Yim et al., 2019).

In general, a significant diurnal variation of $PM_{2.5}$ pollution was observed, possibly due to obvious the local emissions caused by industrial production and human activities for daily living (Amil et al., 2016; Liu et al., 2019a). Particularly, the pollution level was higher during the morning and evening of a normal weekday, with a weakening effect found in the afternoon which may be caused by the co-effects of the boundary layer structure as well as anthropogenic emissions. There was also a seasonal variation of $PM_{2.5}$ pollution across China, indicating a higher level of pollution in winter than summer (Ye et al., 2018; Zhang and Cao, 2015). The $PM_{2.5}$ level of China showed a steady increase from 2004 to 2007, and has since stabilized (Ma et al., 2016); however, there are still frequent $PM_{2.5}$ pollution events in autumn and winter (Song et al., 2017; Yang et al., 2018; Ye et al., 2018; Zhang et al., 2014). In the past few years, the $PM_{2.5}$ concentration in China has decreased significantly as a result of measures introduced across the country that have reduced

multi-pollutant emissions, adjusted energy structure, and increased supply of clean energy (Gui et al., 2019; Yang et al., 2020; Zhang et al., 2019b; Zhang et al., 2020). While $PM_{2.5}$ is still one of the dominant air pollutants across China, surface O_3 pollution in summer has gradually been prominent. Several studies even indicated that O_3 might have replace the role of $PM_{2.5}$ as the primary air pollutant during summer (Li et al., 2019), which has caught the attention of researchers in recent years. For instance, Sun et al. (2016) showed that the observed summertime O_3 at Mt. Tai has increased significantly by 1.7 ppbv yr^{-1} for June and 2.1 ppbv yr^{-1} for July–August during the period of 2003 to 2015. An increase of the maximum daily 8-h average concentration of O_3 (MDA8 O_3) at an annual-average rate of 4.6%, was reported by Fan et al. (2020), albeit with a decrease of the frequency of $PM_{2.5}$ pollution.

The modulations of atmospheric circulation system often lead to changes in meteorological elements, and to a large extent, affect the processes of pollutant formation, transmission and diffusion. And many studies have indicated that $PM_{2.5}$ and O_3 pollution are strongly correlated with local meteorological factors such as temperature, relative humidity (RH) and WS (Huang et al., 2016;Miao et al., 2015; Shu et al., 2019; Tai et al., 2010). Miao et al. (2015) suggested that low boundary layer height (BLH) and stable atmosphere would be an unfavorable condition for the dispersion of winter aerosol pollution over the BTH region. Zhang et al. (2017) found that the majority of O_3 extremes occurred with daily maximum temperature (Tmax) between 300 K and 320 K, minimum RH (RHmin) less than 40%, and minimum WS less than 3 m s^{-1}, through the analysis of extreme O_3 and $PM_{2.5}$ events from historical data (30 years for O_3 and 10 years for $PM_{2.5}$) in the United States. Furthermore, the number of annual extreme $PM_{2.5}$ days was highly positively correlated with the extreme RHmin/Tmax days, and the correlation coefficient between $PM_{2.5}$ and RHmin (Tmax) was highest in urban and suburban (rural) regions. Shi et al. (2020) studied the sensitivity of O_3-8h (O_3 8-hour moving average) and $PM_{2.5}$ associated with meteorological parameters. This study focused on the air pollution and meteorological conditions between January and July, 2013, with a result showing that temperature could have the greatest impact on the daily maximum O_3-8h, while the $PM_{2.5}$ sensitivities are negatively (positively) correlated with temperature ,WS, and BLH (absolute humidity) in most regions of China. Miao et al. (2015) showed that RH is high when aerosol pollution occurs in the BTH region. However, O_3 pollution in China

is more frequent in summer, and the warm and humid flow brought by the East Asian summer monsoon (EASM) induces a hot and humid condition over the summer. Zhao et al. (2019) investigated the RH of O_3 pollution in Shijiazhuang between 15 June and 14 July 2016, and found that the O_3 concentration was higher at moderate humidity (RH average during daytime from 10:00 to 17:00 LT was 40%–50%). Recently, Han et al. (2020) assessed the impacts of local and synoptic meteorological factors on the daily variability of surface O_3 over eastern China. This study revealed that the meteorological factors could explain ~46% of the daily variations of summer surface O_3, Particularly, synoptic factors contributed to ~37% of the overall effects associated with the meteorological factors. Furthermore, six predominant SWPs were identified by the self-organize map and result indicated a weak cyclone system and a southward prevailing wind inducing a positive O_3 anomalies over the eastern China. The abovementioned indicates that the variation of meteorological factors play a non-negligible role in air pollution. Therefore, classification of air pollution according to the meteorological circulation has become particularly important, not least because of its worth when applied to air quality monitoring, forecasting and evaluation (Liu et al., 2019b; Ning et al., 2019; Yang et al., 2018; Zheng et al., 2015).

It has become possible to objectively classify atmospheric circulation conditions using weather data such as GH, sea level pressure, WS and temperature since 1990s, so that the weather mechanism of extreme weather can be better understood and analyzed. Compared with subjective weather classification, the objective approach has been widely used in air pollution research (Miao et al., 2017, 2019; Ning et al., 2018). Miao et al. (2019), based on the daily 900 hPa GH fields during winter in Beijing, identified seven synoptic patterns using an objective approach, and found that the weak northwesterly prevailing winds and strong elevated thermal inversion layer, along with the local emissions of aerosols play a decisive role in the formation of heavy pollution in Beijing; noted also that the southerly prevailing winds can transport the pollutants emitted from southern cities to Beijing. Zheng et al. (2015) studied the relationship between regional pollution and the patterns of large-scale atmospheric circulation over eastern China in October from 2001 to 2010 and identified six pollution types and three clean types. Specifically, weather patterns such as a uniform surface pressure field in eastern China or a steady straight westerly in the middle troposphere, particularly when at the rear of an anticyclone at 850 hPa, were found to be typically responsible for heavy

pollution events. Many studies have suggested a moderating effect of East Asian summer monsoon (EASM) and WPSH on air quality over China (Li et al., 2018; Yin et al., 2019; Zhao et al., 2010). In particular, Li et al. (2018) applied RegCM4-CHEM simulation to analyze the differences of ozone between three strong and weak monsoon years, and found that the concentrations of O_3 over the central and eastern part of China were higher in strong EASM years than that in weak EASM years. The anomalous high-pressure system at 500 hPa, associated with downward dry, hot air and intense solar radiation can enhance the photochemical reactions to elevate the production of tropospheric O_3 (Gong and Liao, 2019; Yin et al., 2019). Furthermore, Zhao & Wang (2017) and Yin et al. (2019) noted that the positive GH anomalies at high latitudes tend to significantly weaken the cold-air advection from the north and result in local high temperatures near the surface in northern China, while the WPSH can transport sufficient water vapor to the YRD region and lead to a decrease in surface O_3. In addition, different subregions can exhibit various distributions of pollutant, even with identical emission scenarios (Li et al., 2019; Saikawa et al., 2017; Zhang et al., 2019a). Also, it is still unclear how the distribution of pollution responds locally to large-scale atmospheric circulation patterns. Due to a variability of local meteorological conditions under the impacts of various synoptic weather types and modulation of large-scale WPSH movement(Li et al., 2018; Wang et al., 2019b; Zhao and Wang, 2017), the causes and consequences of meteorological factors for the formation of compound O_3-$PM_{2.5}$ pollution could be complex. Overall, the mechanism by which the synoptic weather pattern (SWP) modulates the characteristics of O_3-$PM_{2.5}$ compound pollution has yet to be comprehensively described.

In this study, the SWPs corresponding to the co-occurrence O_3-$PM_{2.5}$ pollution during summertime are analyzed, focusing on the eastern China (104°–135°E, 17°–53°N). Then, the synoptic causes of O_3-$PM_{2.5}$ compound pollution, as well as O_3-only pollution, from the perspective of the objective classification of atmospheric circulation patterns, are revealed. The findings are expected to provide a scientific reference for the monitoring, forecasting and evaluation of summertime air pollution in eastern China.

2. Data and methods

The air quality data, including $PM_{2.5}$, NO_2, O_3, and O_3-8h, are from the national 24-h

continuous air quality observation published by the China Environmental Monitoring Station (http://www.cnemc.cn/). Summer hourly data (2015–2018) for 1174 stations were retrieved form an observational network in eastern China (104°–135°E, 17°–53°N), which include the more prominent pollution areas in the eastern urban agglomeration, such as the BTH (113.5°–119.8°E, 36°–42.6°N), YRD (115.3°–122.6°E,27.2°–34.5°N), PRD (112.5°–113.7°E, 21.3°–23.1°N), Guanzhong Plain [GZP (104.6°–112.2°E, 33.3°–36.8°N)], Northeast Megalopolis [NEM (121.2°–131.0°E, 39.8°–47.3°N)] regions (the specific locations of stations and urban agglomerations are shown in Fig. 1a). Surface meteorological data, such as Tmax, precipitation, WS and RH from 611 meteorological observation stations and radiosonde data from 63 stations in eastern China, were obtained from the China National Meteorological Information Center of the China Meteorological Administration (http://data.cma.cn/site/index.html). The BLH was calculated according to the method given by Guo et al. (2016, 2019) (the detailed method can be seen in supplementary materials), and the FLWD [frequency of light wind (< 2 m s^{-1}) days, which can be defined as the ratio between the number of the days with average daily WS lower than 2 m s^{-1} and the total days of each pattern], precipitation frequency (PF, which can be defined as the ratio of the number of the rainy days to the total days under each pattern), and MDA8 O_3 were also counted.

Additionally, for synoptic analysis of particulate matter and O_3 pollution in summer, we use the GH field at 500 hPa, wind and specific humidity field at 850 hPa from the NCEP/NCAR (National Centers for Environmental Prediction/National Center for Atmospheric Research) daily reanalysis dataset on a 2.5° × 2.5° latitude/longitude grid during the study period.

The T-PCA is an objective mathematical computer-based method that can be used to classify the synoptic circulation patterns of regional gridded data in the troposphere at the lower level. Indeed, it is commonly regarded as the most promising weather pattern classification method at present (Huth et al., 2008). Moreover, this approach has been widely used in the studies of aerosols and O_3 pollution-related atmospheric circulation in China (Miao et al., 2017, 2019; Ning et al., 2018, 2019). The T-PCA analysis module of the COST733 software (http://cost733.met.no/) developed by the European Scientific and Technical Research Cooperation, was used to classify the synoptic circulation pattern based on the 500 hPa GH field. The cost733class is a FORTRAN software package consists of several modules for classification, evaluation and comparison of weather and

circulation pattern. First, T-PCA classification of the cost733class performs spatial standardization on weather data. Then split data to 10 subsets and estimates principal components (PCs) of weather information based on singular value decomposition, the PC score for each subset can be calculated after oblique rotation, and compares 10 subsets based on contingency tables to select the subset with highest sum and return its types (Miao et al. 2017). To assess the performance of synoptic classification and determine the number of classes, the explained cluster variance (ECV) is selected in this study (Hoffmann & SchlüNzen, 2013; Ning et al., 2019; Philipp et al., 2014). The detailed information about the ECV is provided in the supplementary document.

Based on the Ambient Air Quality Standards (GB3095-2012) issued by the Ministry of Ecology and Environment of the People's Republic of China, O_3 ($PM_{2.5}$) pollution occurs when the MDA8 O_3 ($PM_{2.5}$ 24-h) concentration exceeds 160 (75) μg m^{-3}. For a region, when haze occurs in more than 50% of the observed sites, the day can be defined as a haze day(Chen and Wang, 2015). In this study, we used the average value of higher 50% O_3 and $PM_{2.5}$ concentrations in each region as the regional values. The specific standard limits of each pollution level are according to their concentration limits based on the Technical Regulation on Ambient Air Quality Index (on trial) (HJ633-2012) issued by the Ministry of Ecology and Environment of the People's Republic of China (Table S1).

Finally, in order to make it clear in the analysis of different weather types of O_3 and $PM_{2.5}$ concentration change, we calculated the average distribution of O_3 and $PM_{2.5}$, as well as the meteorological conditions for each type, and further calculated the anomalous distribution of these variables, i.e., the average of O_3 and $PM_{2.5}$ and the average of the meteorological conditions under the respective patterns minus the average during summertime of 2015–2018, were given as well. The statistical significance was tested with a 0.05 confidence level via analysis of variance, which enabled us to distinguish the significant differences of spatial distribution characteristics between O_3 and $PM_{2.5}$ pollution under four SWPs.

3. Results

3.1 Spatial and temporal distribution of O_3 and $PM_{2.5}$ during summer 2015–2018

Figure 1 shows the summer averaged MDA8 O_3 and $PM_{2.5}$ concentrations at 1174 stations in

the eastern region of China for 2015–2018. Among these stations, the MDA8 O_3 concentration at most stations (795/1174) exceeds 100 μg m^{-3}, of which 45 sites exceed 160 μg m^{-3}. The highest O_3 pollution is found in Zibo, Shandong, with a value of 181.5 μg m^{-3}. The averaged $PM_{2.5}$ at most sites (844/1174) is below 35 μg m^{-3}, while reaches 62.6 μg m^{-3} in Handan, Hebei Province. On the whole, the MDA8 O_3 and $PM_{2.5}$ in the BTH region and its surrounding areas is significantly higher than in other regions; and besides, the level of O_3 in some urban clusters, such as the PRD, YRD, GZP and NEM regions, is particularly higher than that of the surroundings, thus, we focus on analyzing these key areas later.

Figures 2 and 3 respectively show the daily variation of pollution levels of O_3 and $PM_{2.5}$. In recent years, The reduced visibility of haze days weakens the solar radiation reaching the ground and inhibits photochemical reactions from generating O_3 (Li et al., 2019; Zhang et al., 2015), as a result, the concentration of O_3 continues to increase with the mitigation of $PM_{2.5}$ pollution. The days of O_3 pollution in BTH, YRD, PRD, GZP, and NEM regions were 254, 133, 84, 165 and 96 days respectively, while the days of $PM_{2.5}$ pollution were only 93, 8, 0, 2 and 1, of which compound pollution occurred 76, 7, 0, 2, and 0 days according to Chinese standards (the asterisks in Fig. 3 indicate the co-occurred events). China has implemented strict emission control policies and the effects were remarkable. China has implemented strict policies for emission control, and the effects of these policies were remarkable. However, despite a decrease in $PM_{2.5}$ in the last five years, there was also an increase in ozone pollution over China (Fan et al., 2020; Sun et al., 2016), although "double-high" pollution reported on the weather scale has been decreased. As the limit of $PM_{2.5}$ concentration for pollution control is relatively loose in China, previous studies usually referred the interim target 1 (IT-1) of the World Health Organization (WHO) as the standard threshold. Our study pushed forward to the next stage, in which we used IT-2 of WHO (24-h average concentration of $PM_{2.5}$ is 35 μg m^{-3}) as our target limit to count the number of compound pollution days across each region. Based on this target, the pollution days for four SWPs were 194, 52, 16, 47, and 20, respectively (Fig. 3). These results indicated a severe situation of compound pollution that is still deserved a public attention. Thus, the situation of compound pollution is still serious and deserves attention. Overall, the O_3 and $PM_{2.5}$ concentration in eastern China exhibits distinct intraseasonal and interannual variations, indicating that, aside from the changes in emission sources (because it is

considered that inter-seasonal and short-term changes in emission sources are not significant), it may also be regulated by meteorological conditions, which is further analyzed below.

3.2 Objective classification of large-scale synoptic circulation patterns in summer

To analyze the effect of meteorological conditions on the changes of O_3 and $PM_{2.5}$ concentration, it is necessary to statistically analyze the large-scale weather circulation situation in summer. Existing studies have shown that the WPSH (500 hPa GH field with obvious anticyclonic characteristics, and downward flow around the center) in summer prominently regulates the weather and climate of East Asia (Lu, 2002), owing to its various location, shape and intensity (Ding, 1994). A low-level southerly monsoon formed at the periphery of the WPSH can transport warm and humid air from the ocean to East Asia, which might also be responsible for the asymmetric spatial distribution in response to an enhanced WPSH for ground-level O_3, i.e. a decrease in southern China but an increase over northern China (Zhao & Wang, 2017).

Therefore, we used the T-PCA method to objectively classify the weather circulation of the 500-hPa GH field in the summers of 2015–2018, and finally obtained four SWPs related to the movement and development of the WPSH. The location of western ridge point and northern boundary of the WPSH at 500 hPa in Type 1 is around 120°E and 30°N, respectively (Fig. 4a and Table S2). The southwestern flow of this WPSH could transport water vapor to the YRD region, resulting in a southwestward prevailing wind across the YRD region and westward flow from the north of the WPSH forming a convergence area at 850 hPa. These conditions were also associated with high temperature and humidity during the summer with Meiyu season, which Meiyu season is a climate phenomenon with continuous cloudy and rainy days generally occurring during June and July every year in the middle and lower reaches of Yangtze river, Taiwan of China, central/southern Japan, and southern Korea. For Type 2, the westerly trough could deepen as the WPSH shifts northward slightly from Type1 or retreats southeast from Type 3 (Fig. 4b). The southerly wind from the ocean could interact with northern periphery of the WPSH. As a result, the sea-land interaction could interact with the southeastern region across China, while northern China could be mainly controlled by the westerly trough. In compared with Type 2, Type 3 presents the boundary of WPSH in a higher latitude, with a westward extension (Fig. 4c), disintegrating a closed high-pressure

monomer along the eastern coast of China and the main body of the WPSH remains over the ocean (Figs. 4c and S4). This has led to a condition completely controlled by the monomer of the WPSH over the YRD region, resulting a hot and dry weather at the end the rainy season at the beginning of mid-summer. Figure. 4d indicated that the location of the WPSH monomer was more western and northern with respect to other SWPs, controlling the northern China for a long time; the western ridge point was around 95°E and the northern boundary was around 40°N.

Figure 5 presents the daily and annual variations of the SWPs in the summers of 2015–2018. The advance of the WPSH in eastern China occurs in June and July, while gradual withdrawal of the WPSH occurs mainly in August, Type 1 and Type 2 represent normal WPSH characteristics during early and late summer. Type 3 and Type 4 could reflect a split of the WPSH, which mainly occurs in late summer. Consequently, there were167, 117, 52 and 32 days for the Type 1, Type 2, Type 3 and Type 4 over the study period, respectively. Since the WPSH movement is generally affected by the weather phenomenon of its surrounding climatic system (such as typhoons, the Tibetan high, etc.) (Ge et al., 2019; Liu and You, 2020; Shu et al., 2016; Wang et al., 2019), it could result in a short-term southward retreat during the advancement of the WPSH (e.g., around 10 August 2018) and a short-term northward advance during its process of retreat (e.g., 21 and 29 August 2016). In general, the WPSH could represent the evidences of intra-seasonal and interannual changes over China, which will inevitably modulate the weather, climatic and environmental changes in eastern China.

3.3 O_3 and $PM_{2.5}$ pollution characteristics under four SWPs

3.3.1 Spatial characteristics

We calculated the averaged (Fig. S2) and anomalous (Fig. 6) spatial distributions of the MDA8 of O_3 and $PM_{2.5}$ under four SWPs. The O_3 concentration is relatively high in the area north of the Yangtze River under Type 1, and the high values of the MDA8 O_3 are mainly concentrated in the North China Plain (NCP) region, with a total of 100 stations surpassing 160 μg m^{-3}. Type 2 O_3 pollution is slightly weaker than that for Type 1, and the MDA8 O_3 at the 72 sites exceeds 160 μg m^{-3}. The O_3 high-value areas lie mainly in the NCP, GZP and YRD regions under Type 4, and there are 37 stations larger than 160 μg m^{-3}. Of the four SWPs, the lowest overall MDA8 O_3 occurs under

Type 3, with only one site exceeding 160 μg m^{-3} (Figs. S2a-d). It is also found that the regions experiencing significant positive deviations of the MDA8 O_3 from the summer mean are as follows: the BTH, YRD and NEM regions under Type 1, the BTH and GZP regions under Type 2, the middle of the YRD and PRD regions under Type 3, and the YRD, GZP and PRD regions under Type 4 (Figs. 6a-d).

Analogously, Figs. 6e-h shows the anomaly and significance of difference of $PM_{2.5}$ under four weather types, presented as positive anomalies in the south of the BTH and YRD regions under Type 1, in the BTH, GZP and PRD regions under Type 2, and in the GZP and PRD regions under Type 4. Due to the obvious seasonal variations of $PM_{2.5}$ concentration (higher in winter and lower in summer) (Liu et al., 2019a; Miao et al., 2015), no site exceeds 75 μg m^{-3} for the averaged $PM_{2.5}$ concentration. Even so, the level of $PM_{2.5}$ in the BTH region is still significantly higher under four types than that for the other urban agglomerations (Figs. S2e-h).

3.3.2 Pollution pattern differences in key areas

Air pollution is principally found in dense urban areas such as the BTH and YRD regions (Gui et al., 2019; Han et al., 2019), so we took the BTH, PRD, YRD, GZP and NEM regions in the eastern region as key areas, counted the daily anomalies and average variation of O_3 and $PM_{2.5}$ in each key region under different weather patterns (Figs. 7 and S5), and calculated the over-limit ratio in key regions via the stations × days statistics (see Table 1). The diurnal variation of O_3 is more obvious, peaking at about 15:00 (Beijing time), while contrasting diurnal variations of $PM_{2.5}$ are given for different regions. According to Figure 7 and Table 1, the following characteristics can be identified for different urban clusters: (1) in the BTH region, the O_3 concentration of Type 1 and Type 2 is relatively high, their over-standard rates reach 47.1% and 54.2%, and the $PM_{2.5}$ pollution rates of Type 2 and Type 1 reach 18.8% and 16.3%, respectively; (2) in the PRD region, the over-standard rates and concentrations of O_3 and $PM_{2.5}$ is similar under four SWPs; (3) in the YRD region, the O_3 pollution over-limit ratio presents as Type 1 > Type 4 > Type 2 > Type 3, $PM_{2.5}$ pollution largely appears in Type1, and both O_3 and $PM_{2.5}$ in Type 1 are higher than those in the other types; (4) in the GZP region, the O_3 pollution frequency is higher in Type 2 and Type 4, and $PM_{2.5}$ pollution occurs more frequently in Type 2; and (5) in the NEM region, O_3 pollution is always found in Type

1, Type 2 and Type 4, but the over-standard rate is no more than 15% and $PM_{2.5}$ pollution in Type 1 is more than in Type 2.

In summary, Type 1 is prone to the formation of compound pollution of O_3-$PM_{2.5}$ (that is, when the ground MDA8 O_3 concentration exceeds 160 μg m^{-3}, the $PM_{2.5}$ concentration also exceeds 75 μg m^{-3}) in the area from BTH to northern YRD regions (Fig. S11), which can be denoted as "BTH – NYRD O_3-$PM_{2.5}$ compound pollution". Similarly, Type 2 can also be denoted as "BTH O_3-$PM_{2.5}$ compound pollution", Type 3 as "BTH – YRD – PRD O_3-only pollution", and Type 4 as "BTH – GZP – YRD – PRD O_3-only pollution" (Fig.12).

3.4 Analysis of potential meteorological factors

Therefore, to explore the meteorological causes of O_3 and $PM_{2.5}$ pollution, we analyzed the distribution of the average and anomalies for Tmax, RH, PF, BLH and FLWD under four SWPs (Figs. S6, S7, 8 and 9). Under the influence of the EASM, over 80% of the stations experience high temperatures (Tmax > 27℃) in each SWP, although the anomaly of Tmax in Type 1 (early summer) presents negative (Fig. 8a). Type 1 is characterized by humid condition in the southern area and dry condition in the northern region owing to an extensive southwestern flow of the WPSH, resulting in a rain belt found in southeastern coastal area such as PRD and YRD regions. Type 2 is associated with meridional flow and dry and wet anomalies in northern China, resulting in a rain band locating at the central areas of between BTH and YRD regions due to the northern advance of the WPSH compared with Type 1. Furthermore, there is a greater RH for most of the study sites under Type 3 and Type 4, possibly a result of the shifted rain belt in the BTH and NEM regions under Type 3 once the northern boundary of the WPSH reaching at 37.5°N, and an occurrence of heavy precipitation across the western PRD region as well as central areas of between BTH and YRD regions under Type 4 (Fig. S6).

In terms of their anomalous spatial distribution, the positive anomalies of Tmax are located in the southern region of Type 3 and most of the eastern region of Type 4; and since Type 1 always appears in early summer, most areas are negative (Figs. 8a–d). For RH, Types 2, 3 and 4 are negative for the south and positive for the north, while Type 1 is opposite (Figs. 8e–h). PF is characterized by positive anomalies in the area south of the Yangtze River under Type 1, in the YRD region under

Type 2, in the BTH and NEM regions under Type 3, and in the area between the BTH and YRD regions under Type 4 (Figs. 8i–l). As can be seen from Fig. 9, when the BLH at 14:00 (BJT) has a positive anomaly, on the contrary FLWD has a negative anomaly (e.g., BTH in Type 1), which indicates the higher BLH, the lower FLWD, the more conducive to the diffusion of pollutants, otherwise, lower BLH and higher FLWD (such as BTH in Type 2) do not support the diffusion. After further inspection of Fig. S7, we found the YRD region in Type 1, the YRD in Type 2, the BTH and PRD regions in Type 3 and 4 have shallow BLHs and high FLWDs, which is detrimental to the transportation of pollution in these areas, thus corresponding to high levels of pollution under these weather patterns. But in some higher BLH areas, there were also more serious pollution, such as BTH under Type 1, which we will discuss next.

3.5 Potential implications of NO_2

Photochemical production of O_3 mainly involve emissions of VOCs and NO_x from anthropogenic, biogenic and biomass burning sources (Deng et al., 2019; Gvozdić et al., 2011; Sillman, 2002). The photochemical reaction of NO, NO2, and O_3 in the troposphere form a closed system(Yu et al., 2020), and this photochemical cycle of NOx and O_3 is the basis of photochemical processes in the troposphere. Oxidant (Ox, $Ox=O_3+NO_2$), a conservative quantity over short time scales, is defined as a parameter to evaluate the photochemical processes due to the unstable nature of NO, it can quickly react with the equivalent amount of O_3 to generate NO_2 (Kley et al., 1994). In order to compare the photochemical reaction efficiency of five urban clusters under different SWPs, Figure 10 can present the daily variation of NO_2 and Ox. These include daily variations of NO_2 showing two peaks during a day, including a first peak at the morning and an second peak associated with traffic emissions in the evening (Xie et al., 2016; Yu et al., 2020). As we found the lowest point of NO_2 at 15:00 (BJT), and NO_2 can be photolyzed to produce O_3 during the day, this study assumed that this particular time was the peak formation ozone across the study areas. As NO_2 was consumed through a photochemical reaction with the involvement of other precursors to produce a large amount of O_3, Ox could form a peak during the afternoon. In particular, abundant sunlight in summer is beneficial to the photochemical reaction process, but since most parts of eastern China are in a subtropical climate with the same period of rain and heat, the existence of the rainy season will

inevitably inhibit the summer photochemical process. Under different SWP, the photochemical reaction over each area has an obvious relationship with the rain belt. For example, the rainy season in BTH and NEM areas mainly occurs in Type 3, and the Ox of Type 3 in this area is significantly lower than other SWPs.

400

4. Discussion

In the last section, we have discussed how the SWPs and local meteorological factors modify summer O_3 and $PM_{2.5}$ pollution. However, how does the boundary layer structure interact with the co-occurrence O_3-$PM_{2.5}$ pollution? In order to address this question, we conducted a further analysis. As mentioned, co-occurrence of O_3 and $PM_{2.5}$ pollution mainly occurs in the BTH – NYRD under Type 1 and BTH under Type 2. Lower WS and its negative anomalies at lower boundary layer over BTH– NYRD under Type 1 and over BTH under Type 2 may not enhance the diffusion of air pollutants (Fig. S8). In contrast, moderate RH and its negative anomalies might favor the formation of compound pollution. Downward vertical motion and negative anomalies could also stabilize the atmospheric characteristic of boundary layer (Fig. S9). Furthermore, we summarized boundary layer structure, precipitation, and ground-level wind flow across the BTH region. Based on the characteristics, we separately defined Type 1 and Type 2 into clean (both concentrations of the O_3 and $PM_{2.5}$ are less than polluted level) and compound pollution periods (Figs. 11 and S10-S11). Particularly, Type1 has a significantly warmer temperature over the boundary layer during the compound pollution period of BTH region than that of the clean period. The daytime BLH under compound pollution condition was also higher than that of the clean condition. In addition, there were different directions of prevailing during the two periods, which prevailing winds during the compound pollution period were usually southward and could be driven by air pollutants transported from the southern plains (Fig. 11; see also Miao et al., 2019b, 2020). Co-influencing by the topographical effect of the northern mountainous areas, air pollutants could be trapped in the BTH region. In comparison, although there was southward wind prevailing in the BTH region (Figs. 11 and S11), the rain belt also located in the southern area of BTH might lead to the potential removal of $PM_{2.5}$ (Fig. 9j). Therefore, compound pollution across the BTH region might mainly be due to local emissions of air pollutants.

In summary, the different SWPs can modulate the regional variability of summertime O_3 and $PM_{2.5}$ and their causes in summer as follows:

(1) Type 1: The area to the north of the YRD under Type 1 is controlled by the westerly zone in the north of the WPSH at 500 hPa. Under the conditions of high temperature (Tmax > 27℃), moderate humidity (RH ~60%), and low PF, photochemical reactions are largely promoted to cause severe O_3 pollution. Meanwhile, BTH– NYRD is located in front of the westerly trough, under the influence of the warm and humid air of the WPSH, and so the hygroscopic growth of fine particulates will cause a certain amount of $PM_{2.5}$ pollution, becoming O_3-$PM_{2.5}$ compound pollution (Fig. 12). Particularly, the prevailing southerly winds in the boundary layer can transport the pollutants emitted from southern cities to BTH, atmospheric stratification is stable when the air mass is sinking, compound pollution may be especially severe. Although relative higher BLH occurred in the BTH, the prevailing southerly winds in the boundary layer has increased pollution more. In Figure S12, we counted the number and probability of occurrence of compound pollution days in each site in summer during 2015-2018, indicating that high occurrence probability (maximum values can approach 46.7%) of compound pollution appeared in the Northern China plain (to the north of 32°N). About 55.6% of compound pollution occurrence days at all sites occurred under Type 1.

(2) Type 2: As the northern advance of WPSH from Type 1 or the retreat from Type 3 or Type 4, and the northern region is still controlled by the westerly zone. Ozone pollution is severe under the meteorological conditions of high temperature, moderate humidity, and few precipitations. The $PM_{2.5}$ in the BTH region, which is located in front of the westerly trough, is high since the shallow boundary layer and low wind frequency are unfavorable for pollutant diffusion. Therefore, O_3-$PM_{2.5}$ compound pollution can also be rather frequent (Fig. 12). About 33.8% of compound pollution occurrence days at all sites occurred under Type 2 in summer during 2015-2018.

(3) Type 3: High temperature, low humidity and few precipitations over the YRD region tend to generate a large amount of O_3, while the positive BLH and negative FLWD anomalies are unfavorable to O_3 accumulation. On the other hand, summer typhoon activities might weaken the WPSH intensity over the YRD region, leading to the eastward retreat and northward shift of the WPSH. As a result, high WS across coastal areas could ease the ground-level O_3 pollution (Shu et

al., 2016). For the BTH and PRD regions, high PF tends to suppress the O_3 production. Only 6.8% of the compound pollution occurrence days at all sites occurred under Type 3, in accordant with light O_3-only pollution over the areas of the BTH, YRD and PRD (Fig. 12).

(4) Type 4: High temperatures, medium-high humidity and few precipitations in the GZP and PRD regions can cause O_3-$PM_{2.5}$ compound pollution, but $PM_{2.5}$ pollution in both regions are not heavy, which is possibly in relation to local lower pollutant emissions. The probability of compound pollution occurrence under Type 4 is about 5.1%. Under the control of the WPSH, there are strong photochemical reactions at high temperatures and little rainfall in some eastern region (such as the northern BTH, YRD), which is also conducive to O_3 generation (Fig. 12). Meanwhile, relative to Type 1, O_3 pollution is lighter in the BTH, due to the differences of RH, BLH and FLWD.

5 Conclusions

In this study, T-PCA, an objective classification method, was applied to classify the 500-hPa weather circulation pattern as four SWPs in the summers of 2015–2018. It was found that these four SWPs are closely related to the development of the WPSH. The spatial and temporal distribution characteristics of O_3 and $PM_{2.5}$ pollution in eastern China under four SWPs were analyzed to regulate and differentiate O_3 and $PM_{2.5}$ pollution in key areas. We find two synoptic patterns are prone to lead to co-occurrence of O_3 and $PM_{2.5}$ pollution: in BTH– NYRD under Type 1 and BTH under Type 2 are associated with the double high level of O_3 and $PM_{2.5}$. The probabilities of compound pollution at all sites under Type 1, 2, 3, and 4 are 54.3%, 33.8%, 6.8%, and 5.1% respectively.

Type 1 weather pattern appears frequently in early summer, with a stable WPSH ridge axis at about 22°N, and the warm and humid air brought by the WPSH reaches the area south of the Yangtze River, where a high temperature and high humidity Meiyu season is formed, the high humidity would suppress the photochemical reaction of O_3 generation. Meanwhile, the north of China is controlled by a low-pressure trough at 500 hPa with high temperatures and little rain. The hygroscopic growth of $PM_{2.5}$ occurs in the corresponding area in front of the trough with a small amount of water vapor transported by the WPSH, causing compound pollution of O_3 and $PM_{2.5}$ in the BTH– NYRD. In addition, the prevailing southerly winds in the boundary layer can transport

the pollutants emitted from southern cities to the BTH region, and the atmospheric stratification is stable when the air mass is sinking. Thus, the compound pollution can be severe. In general, the synoptic circulation in the boundary layer might be responsible for the concentration of pollutants under this SWPs.

Under Type 2, the WPSH shifts northwards from Type 1 or retreats southwards from Type 3 or Type 4 to 32.5°N, with the meridional deepening of the East Asian major trough at 500 hPa, and thus warm and humid airstreams are brought to the Northern China (e.g., the BTH region), gradually elevating temperatures and humidity. Although positive RH anomaly promotes hygroscopic growth of the $PM_{2.5}$, water vapor absorbs solar radiation leading to reduced O_3 formation by contrast. As a result, the probability of double high level of O_3 and $PM_{2.5}$ under Type 2 is less than Type 1, the extent of compound pollution in Type 2 is also narrowed, which mainly located in the BTH. On the other hand, weak precipitation, shallow boundary layer and low wind speed in the BTH tend to create favorable conditions for pollution maintenance. In spite of the southerly winds over the BTH, the precipitation in southern cities has reduced pollutants and reduced horizontal transport. The meteorological factors might be responsible for the accumulation of compound pollution.

In general, the location of the WPSH is tightly associated with O_3 pollution in eastern China, and the changes of meteorological conditions in different regions affected by the WPSH can induce significant regional differences in O_3 and $PM_{2.5}$ pollution. On one hand, the appropriate warm moist flow brought by the WPSH can promote hygroscopic growth of the fine particulate matter in some local areas (i.e., BTH-NYRD under Type 1 and BTH under Type 2), resulting in the increase of PM2.5 concentrations; On the other hand, transboundary O_3 was transported to these local areas at the same time, which may contribute to form the co-occurring surface O_3 and $PM_{2.5}$ pollution More importantly, the effects of various large-scale weather circulation patterns on the O_3-$PM_{2.5}$ compound pollution and their corresponding physical and chemical processes, have been clarified, which has important scientific reference value in summer air-quality forecasts, as well as assessment and policy-making services.

Besides, although this study emphasized the important impacts of large-scale synoptic drivers of co-occurring summertime O_3 and $PM_{2.5}$ pollution in eastern China, the presences of $PM_{2.5}$ may play a role in radiation forcing to reduce O_3, the interaction between O_3 and $PM_{2.5}$ which deserves

further exploration to better comprehend the mechanism of O_3-$PM_{2.5}$ compound pollution in the future work.

Data availability

Hourly $PM_{2.5}$, NO_2, O_3, and O_3-8h data is published by the China Environmental Monitoring Station (http://www.cnemc.cn/). Surface meteorological data, such as Tmax, precipitation, WS and RH, radiosonde data can be obtained from the China National Meteorological Information Center of the China Meteorological Administration (http://data.cma.cn/site/index.html). The NCEP/NCAR daily reanalysis dataset can be download from https://psl.noaa.gov/data/gridded/data.ncep.reanalysis.html.

Author contributions

L. Zong: Methodology, Data Curation, Formal Analysis, Writing- Original draft preparation, Results Discussion, Writing- Reviewing and Editing; Y. Yang: Conceptualization, Methodology, Formal Analysis, Results Discussion, Writing- Reviewing and Editing; M. Gao, H. Wang, P. Wang, L. Wang, H. Zhang, G. Ning, C. Liu, Y. Li, Z. Gao: Results Discussion, Comments, Writing- Reviewing and Editing.

Competing interests

The authors declare that they have no conflict of interests.

Acknowledgments

This study was jointly funded by supported by the National Key Research and Development Program of China (2018YFC1506502) and the National Natural Science Foundation of China (41871029).

References

Amil, N., Latif, M. T., Khan, M. F. and Mohamad, M.: Seasonal variability of PM2.5composition and sources in the Klang Valley urban-industrial environment, Atmos. Chem. Phys., 16(8),

5357–5381, doi:10.5194/acp-16-5357-2016, 2016.

Cai, W., Li, K., Liao, H., Wang, H. and Wu, L.: Weather conditions conducive to Beijing severe haze more frequent under climate change, Nat. Clim. Chang., 7(4), 257–262, doi:10.1038/nclimate3249, 2017.

Chen, C., Saikawa, E., Comer, B., Mao, X. and Rutherford, D.: Ship Emission Impacts on Air Quality and Human Health in the Pearl River Delta (PRD) Region, China, in 2015, With Projections to 2030, GeoHealth, 3(9), 284–306, doi:10.1029/2019GH000183, 2019.

Chen, H. and Wang, H.: Haze days in North China and the associated atmospheric circulations based on daily visibility data from 1960 to 2012, J. Geophys. Res., 120(12), 5895–5909, doi:10.1002/2015JD023225, 2015.

Cohen, A. J., Brauer, M., Burnett, R., Anderson, H. R., Frostad, J., Estep, K., Balakrishnan, K., Brunekreef, B., Dandona, L., Dandona, R., Feigin, V., Freedman, G., Hubbell, B., Jobling, A., Kan, H., Knibbs, L., Liu, Y., Martin, R., Morawska, L., Pope, C. A., Shin, H., Straif, K., Shaddick, G., Thomas, M., van Dingenen, R., van Donkelaar, A., Vos, T., Murray, C. J. L. and Forouzanfar, M. H.: Estimates and 25-year trends of the global burden of disease attributable to ambient air pollution: an analysis of data from the Global Burden of Diseases Study 2015, Lancet, 389(10082), 1907–1918, doi:10.1016/S0140-6736(17)30505-6, 2017.

Day, D. B., Xiang, J., Mo, J., Li, F., Chung, M., Gong, J., Weschler, C. J., Ohman-Strickland, P. A., Sundell, J., Weng, W., Zhang, Y. and Zhang, J. J.: Association of ozone exposure with cardiorespiratory pathophysiologic mechanisms in healthy adults, JAMA Intern. Med., 177(9), 1344–1353, doi:10.1001/jamainternmed.2017.2842, 2017.

Deng, Y., Li, J., Li, Y., Wu, R. and Xie, S.: Characteristics of volatile organic compounds, NO2, and effects on ozone formation at a site with high ozone level in Chengdu, J. Environ. Sci. (China), 75(2), 334–345, doi:10.1016/j.jes.2018.05.004, 2019.

Ding, Y.: The Summer Monsoon in East Asia, in Monsoons over China, pp. 1–90., 1994.

Du, Y., Wan, Q., Liu, H., Liu, H., Kapsar, K. and Peng, J.: How does urbanization influence PM 2.5 concentrations? Perspective of spillover effect of multi-dimensional urbanization impact, J. Clean. Prod., 220, 974–983, doi:10.1016/j.jclepro.2019.02.222, 2019.

Fan, H., Zhao, C. and Yang, Y.: A comprehensive analysis of the spatio-temporal variation of urban

air pollution in China during 2014–2018, Atmos. Environ., 220(November), 117066, doi:10.1016/j.atmosenv.2019.117066, 2020.

Ge, J., You, Q. and Zhang, Y.: Effect of Tibetan Plateau heating on summer extreme precipitation in eastern China, Atmos. Res., 218, 364–371, doi:10.1016/j.atmosres.2018.12.018, 2019.

Gong, C. and Liao, H.: A typical weather pattern for ozone pollution events in North China, Atmos. Chem. Phys., 19(22), 13725–13740, doi:10.5194/acp-19-13725-2019, 2019.

Gui, K., Che, H., Wang, Y., Wang, H., Zhang, L., Zhao, H., Zheng, Y., Sun, T. and Zhang, X.: Satellite-derived PM2.5 concentration trends over Eastern China from 1998 to 2016: Relationships to emissions and meteorological parameters, Environ. Pollut., 247, 1125–1133, doi:10.1016/j.envpol.2019.01.056, 2019.

Guo, J., Miao, Y., Zhang, Y., Liu, H., Li, Z., Zhang, W., He, J., Lou, M., Yan, Y., Bian, L. and Zhai, P.: The climatology of planetary boundary layer height in China derived from radiosonde and reanalysis data, Atmos. Chem. Phys., 16(20), 13309–13319, doi:10.5194/acp-16-13309-2016, 2016.

Guo, J., Li, Y., Cohen, J. B., Li, J., Chen, D., Xu, H., Liu, L., Yin, J., Hu, K. and Zhai, P.: Shift in the Temporal Trend of Boundary Layer Height in China Using Long-Term (1979–2016) Radiosonde Data, Geophys. Res. Lett., 46(11), 6080–6089, doi:10.1029/2019GL082666, 2019.

Gvozdić, V., Kovač-Andrić, E. and Brana, J.: Influence of Meteorological Factors NO2, SO2, CO and PM10 on the Concentration of O3 in the Urban Atmosphere of Eastern Croatia, Environ. Model. Assess., 16(5), 491–501, doi:10.1007/s10666-011-9256-4, 2011.

Han, H., Liu, J., Shu, L., Wang, T. and Yuan, H.: Local and synoptic meteorological influences on daily variability in summertime surface ozone in eastern China, Atmos. Chem. Phys., 20(1), 203–222, doi:10.5194/acp-20-203-2020, 2020.

Hoffmann, P. and Heinke SchlüNzen, K.: Weather pattern classification to represent the urban heat island in present and future climate, J. Appl. Meteorol. Climatol., 52(12), 2699–2714, doi:10.1175/JAMC-D-12-065.1, 2013.

Huang, X., Ding, A., Liu, L., Liu, Q., Ding, K., Nie, W., Xu, Z., Chi, X., Wang, M., Sun, J., Guo, W. and Fu, C.: Effects of aerosol-radiation interaction on precipitation during biomass-burning season in East China, Atmos. Chem. Phys. Discuss., (April), 1–37, doi:10.5194/acp-2016-272,

2016.

Huth, R., Beck, C., Philipp, A., Demuzere, M., Ustrnul, Z., Cahynová, M., Kyselý, J. and Tveito, O. E.: Classifications of atmospheric circulation patterns: Recent advances and applications, Ann. N. Y. Acad. Sci., 1146, 105–152, doi:10.1196/annals.1446.019, 2008.

Ji, X., Yao, Y. and Long, X.: What causes PM2.5 pollution? Cross-economy empirical analysis from socioeconomic perspective, Energy Policy, 119(April), 458–472, doi:10.1016/j.enpol.2018.04.040, 2018.

Kley, D., Geiss, H. and Mohnen, V. A.: Tropospheric ozone at elevated sites and precursor emissions in the United States and Europe, Atmos. Environ., 28(1), 149–158, doi:10.1016/1352-2310(94)90030-2, 1994.

Li, K., Jacob, D. J., Liao, H., Zhu, J., Shah, V., Shen, L., Bates, K. H., Zhang, Q. and Zhai, S.: A two-pollutant strategy for improving ozone and particulate air quality in China, Nat. Geosci., 12(11), 906–910, doi:10.1038/s41561-019-0464-x, 2019.

Li, M., Wang, L., Liu, J., Gao, W., Song, T., Sun, Y., Li, L., Li, X., Wang, Y., Liu, L., Daellenbach, K. R., Paasonen, P. J., Kerminen, V. M., Kulmala, M. and Wang, Y.: Exploring the regional pollution characteristics and meteorological formation mechanism of PM2.5 in North China during 2013–2017, Environ. Int., 134(November 2019), 105283, doi:10.1016/j.envint.2019.105283, 2020.

Li, S., Wang, T., Huang, X., Pu, X., Li, M., Chen, P., Yang, X. Q. and Wang, M.: Impact of East Asian Summer Monsoon on Surface Ozone Pattern in China, J. Geophys. Res. Atmos., 123(2), 1401–1411, doi:10.1002/2017JD027190, 2018.

Liu, H., Tian, H., Zhang, K., Liu, S., Cheng, K., Yin, S., Liu, Y., Liu, X., Wu, Y., Liu, W., Bai, X., Wang, Y., Shao, P., Luo, L., Lin, S., Chen, J. and Liu, X.: Seasonal variation, formation mechanisms and potential sources of PM2.5 in two typical cities in the Central Plains Urban Agglomeration, China, Sci. Total Environ., 657, 657–670, doi:10.1016/j.scitotenv.2018.12.068, 2019a.

Liu, J. and You, Q.: A diagnosis of the interannual variation of the summer hydrometeor based on ERA-interim over Eastern China, Atmos. Res., 231(October 2018), 104654, doi:10.1016/j.atmosres.2019.104654, 2020.

Liu, N., Zhou, S., Liu, C. and Guo, J.: Synoptic circulation pattern and boundary layer structure associated with PM2.5 during wintertime haze pollution episodes in Shanghai, Atmos. Res., 228(46), 186–195, doi:10.1016/j.atmosres.2019.06.001, 2019b.

Lu, R.: Indices of the Summertime Western North Pacific Subtropical High, Adv. Atmos. Sci., 19(6), 1004–1028, doi:10.1007/s00376-002-0061-5, 2002.

Ma, Z., Hu, X., Sayer, A. M., Levy, R., Zhang, Q., Xue, Y., Tong, S., Bi, J., Huang, L. and Liu, Y.: Satellite-based spatiotemporal trends in PM2.5 concentrations: China, 2004-2013, Environ. Health Perspect., 124(2), 184–192, doi:10.1289/ehp.1409481, 2016.

Miao, Y., Hu, X.-M., Liu, S., Qian, T., Xue, M., Zheng, Y. and Wang, S.: Seasonal variation of local atmospheric circulations and boundary layer structure in the Beijing-Tianjin-Hebei region and implications for air quality., J. Adv. Model. Earth Syst., 7, 1602–1626, doi:10.1002/2015ms000522, 2015.

Miao, Y., Guo, J., Liu, S., Liu, H., Li, Z., Zhang, W. and Zhai, P.: Classification of summertime synoptic patterns in Beijing and their associations with boundary layer structure affecting aerosol pollution, Atmos. Chem. Phys., 17(4), 3097–3110, doi:10.5194/acp-17-3097-2017, 2017.

Miao, Y., Liu, S. and Huang, S.: Synoptic pattern and planetary boundary layer structure associated with aerosol pollution during winter in Beijing, China, Sci. Total Environ., 682, 464–474, doi:10.1016/j.scitotenv.2019.05.199, 2019.

Miao, Y., Che, H., Zhang, X. and Liu, S.: Relationship between summertime concurring PM2.5 and O3 pollution and boundary layer height differs between Beijing and Shanghai, China, Environ. Pollut., doi:10.1016/j.envpol.2020.115775, 2020.

Ning, G., Wang, S., Yim, S. H. L., Li, J., Hu, Y., Shang, Z., Wang, J. and Wang, J.: Impact of low-pressure systems on winter heavy air pollution in the northwest Sichuan Basin, China, Atmos. Chem. Phys., 18(18), 13601–13615, doi:10.5194/acp-18-13601-2018, 2018.

Ning, G., Yim, S. H. L., Wang, S., Duan, B., Nie, C., Yang, X., Wang, J. and Shang, K.: Synergistic effects of synoptic weather patterns and topography on air quality: a case of the Sichuan Basin of China, Clim. Dyn., 53(11), 6729–6744, doi:10.1007/s00382-019-04954-3, 2019.

Philipp, A., Beck, C., Esteban, P., Krennert, T., Lochbihler, K., Spyros, P., Pianko-kluczynska, K.,

Post, P., Alvarez, R., Spekat, A. and Streicher, F.: Cost733 user guide., 2014.

Saikawa, E., Kim, H., Zhong, M., Avramov, A., Zhao, Y., Janssens-Maenhout, G., Kurokawa, J. I., Klimont, Z., Wagner, F., Naik, V., Horowitz, L. W. and Zhang, Q.: Comparison of emissions inventories of anthropogenic air pollutants and greenhouse gases in China, Atmos. Chem. Phys., 17(10), 6393–6421, doi:10.5194/acp-17-6393-2017, 2017.

Shi, Z., Huang, L., Li, J., Ying, Q., Zhang, H. and Hu, J.: Sensitivity Analysis of the Surface Ozone and Fine Particulate Matter to Meteorological Parameters in China, Atmos. Chem. Phys. Discuss., 2020, 1–29, doi:10.5194/acp-2020-173, 2020.

Shu, L., Xie, M., Wang, T., Gao, D., Chen, P., Han, Y., Li, S., Zhuang, B. and Li, M.: Integrated studies of a regional ozone pollution synthetically affected by subtropical high and typhoon system in the Yangtze River Delta region, China, Atmos. Chem. Phys., 16(24), 15801–15819, doi:10.5194/acp-16-15801-2016, 2016.

Shu, L., Wang, T., Xie, M., Li, M., Zhao, M., Zhang, M. and Zhao, X.: Episode study of fine particle and ozone during the CAPUM-YRD over Yangtze River Delta of China: Characteristics and source attribution, Atmos. Environ., 203(July 2018), 87–101, doi:10.1016/j.atmosenv.2019.01.044, 2019.

Sillman, S.: Chapter 12 The relation between ozone, NOx and hydrocarbons in urban and polluted rural environments, Dev. Environ. Sci., 1(C), 339–385, doi:10.1016/S1474-8177(02)80015-8, 2002.

Song, C., Wu, L., Xie, Y., He, J., Chen, X., Wang, T., Lin, Y., Jin, T., Wang, A., Liu, Y., Dai, Q., Liu, B., Wang, Y. nan and Mao, H.: Air pollution in China: Status and spatiotemporal variations, Environ. Pollut., 227, 334–347, doi:10.1016/j.envpol.2017.04.075, 2017.

Sun, L., Xue, L., Wang, T., Gao, J., Ding, A., Cooper, O. R., Lin, M., Xu, P., Wang, Z., Wang, X., Wen, L., Zhu, Y., Chen, T., Yang, L., Wang, Y., Chen, J. and Wang, W.: Significant increase of summertime ozone at Mount Tai in Central Eastern China, Atmos. Chem. Phys., 16(16), 10637–10650, doi:10.5194/acp-16-10637-2016, 2016.

Tai, A. P. K., Mickley, L. J. and Jacob, D. J.: Correlations between fine particulate matter (PM2.5) and meteorological variables in the United States: Implications for the sensitivity of PM2.5 to climate change, Atmos. Environ., 44(32), 3976–3984, doi:10.1016/j.atmosenv.2010.06.060,

2010.

Wang, H. J. and Chen, H. P.: Understanding the Recent Trend of Haze Pollution in Eastern China: Roles of Climate Change, Atmos. Chem. Phys. Discuss., 2016(January), 1–18, doi:10.5194/acp-2015-1009, 2016.

Wang, T., Zhong, Z., Sun, Y. and Wang, J.: Impacts of tropical cyclones on the meridional movement of the western Pacific subtropical high, Atmos. Sci. Lett., 20(5), 1–8, doi:10.1002/asl.893, 2019.

Xie, M., Zhu, K., Wang, T., Chen, P., Han, Y., Li, S., Zhuang, B. and Shu, L.: Temporal characterization and regional contribution to O 3 and NO x at an urban and a suburban site in Nanjing, China, Sci. Total Environ., 551–552(x), 533–545, doi:10.1016/j.scitotenv.2016.02.047, 2016.

Yang, Y., Zheng, X., Gao, Z., Wang, H., Wang, T., Li, Y., Lau, G. N. C. and Yim, S. H. L.: Long-Term Trends of Persistent Synoptic Circulation Events in Planetary Boundary Layer and Their Relationships With Haze Pollution in Winter Half Year Over Eastern China, J. Geophys. Res. Atmos., 123(19), 10,991-11,007, doi:10.1029/2018JD028982, 2018.

Yang, Y., Zheng, Z., Yim, S. Y. L., Roth, M., Ren, G., Gao, Z., Wang, T., Li, Q., Shi, C., Ning, G. and Li, Y.: PM2.5 Pollution Modulates Wintertime Urban Heat Island Intensity in the Beijing-Tianjin-Hebei Megalopolis, China, Geophys. Res. Lett., 47(1), 0–3, doi:10.1029/2019GL084288, 2020.

Ye, W. F., Ma, Z. Y. and Ha, X. Z.: Spatial-temporal patterns of PM2.5 concentrations for 338 Chinese cities, Sci. Total Environ., 631–632, 524–533, doi:10.1016/j.scitotenv.2018.03.057, 2018.

Yim, S. H. L., Wang, M., Gu, Y., Yang, Y., Dong, G. and Li, Q.: Effect of Urbanization on Ozone and Resultant Health Effects in the Pearl River Delta Region of China, J. Geophys. Res. Atmos., 124(21), 11568–11579, doi:10.1029/2019JD030562, 2019.

Yin, Z., Cao, B. and Wang, H.: Dominant patterns of summer ozone pollution in eastern China and associated atmospheric circulations, Atmos. Chem. Phys., 19(22), 13933–13943, doi:10.5194/acp-19-13933-2019, 2019.

Yu, S., Yin, S., Zhang, R., Wang, L., Su, F., Zhang, Y. and Yang, J.: Spatiotemporal characterization and regional contributions of O3 and NO2: An investigation of two years of monitoring data

in Henan, China, J. Environ. Sci. (China), 90(November), 29–40, doi:10.1016/j.jes.2019.10.012, 2020.

Zhang, C., Liu, C., Hu, Q., Cai, Z., Su, W., Xia, C., Zhu, Y., Wang, S. and Liu, J.: Satellite UV-Vis spectroscopy: implications for air quality trends and their driving forces in China during 2005–2017, Light Sci. Appl., 8(1), doi:10.1038/s41377-019-0210-6, 2019a.

Zhang, H., Wang, Y., Park, T. W. and Deng, Y.: Quantifying the relationship between extreme air pollution events and extreme weather events, Atmos. Res., 188, 64–79, doi:10.1016/j.atmosres.2016.11.010, 2017.

Zhang, Q., Zheng, Y., Tong, D., Shao, M., Wang, S., Zhang, Y., Xu, X., Wang, J., He, H., Liu, W., Ding, Y., Lei, Y., Li, J., Wang, Z., Zhang, X., Wang, Y., Cheng, J., Liu, Y., Shi, Q., Yan, L., Geng, G., Hong, C., Li, M., Liu, F., Zheng, B., Cao, J., Ding, A., Gao, J., Fu, Q., Huo, J., Liu, B., Liu, Z., Yang, F., He, K. and Hao, J.: Drivers of improved PM2.5 air quality in China from 2013 to 2017, Proc. Natl. Acad. Sci. U. S. A., 116(49), 24463–24469, doi:10.1073/pnas.1907956116, 2019b.

Zhang, R. H., Li, Q. and Zhang, R. N.: Meteorological conditions for the persistent severe fog and haze event over eastern China in January 2013, Sci. China Earth Sci., 57(1), 26–35, doi:10.1007/s11430-013-4774-3, 2014.

Zhang, W., Wang, H., Zhang, X., Peng, Y., Zhong, J., Wang, Y. and Zhao, Y.: Evaluating the contributions of changed meteorological conditions and emission to substantial reductions of PM2.5 concentration from winter 2016 to 2017 in Central and Eastern China, Sci. Total Environ., 716, 136892, doi:10.1016/j.scitotenv.2020.136892, 2020.

Zhang, Y. L. and Cao, F.: Fine particulate matter (PM 2.5) in China at a city level, Sci. Rep., 5(2014), 1–12, doi:10.1038/srep14884, 2015.

Zhang, Z., Zhang, X., Gong, D., Quan, W., Zhao, X., Ma, Z. and Kim, S. J.: Evolution of surface O3 and PM2.5 concentrations and their relationships with meteorological conditions over the last decade in Beijing, Atmos. Environ., 108, 67–75, doi:10.1016/j.atmosenv.2015.02.071, 2015.

Zhang, Z., Zhang, X., Gong, D., Kim, S. J., Mao, R. and Zhao, X.: Possible influence of atmospheric circulations on winter haze pollution in the Beijing-Tianjin-Hebei region, northern China,

Atmos. Chem. Phys., 16(2), 561–571, doi:10.5194/acp-16-561-2016, 2016.

Zhao, C., Wang, Y., Yang, Q., Fu, R., Cunnold, D. and Choi, Y.: Impact of East Asian summer monsoon on the air quality over China: View from space, J. Geophys. Res. Atmos., 115(9), 1–12, doi:10.1029/2009JD012745, 2010.

Zhao, W., Tang, G., Yu, H., Yang, Y., Wang, Y., Wang, L., An, J., Gao, W., Hu, B., Cheng, M., An, X., Li, X. and Wang, Y.: Evolution of boundary layer ozone in Shijiazhuang, a suburban site on the North China Plain, J. Environ. Sci. (China), 83, 152–160, doi:10.1016/j.jes.2019.02.016, 2019.

Zhao, Z. and Wang, Y.: Influence of the West Pacific subtropical high on surface ozone daily variability in summertime over eastern China, Atmos. Environ., 170, 197–204, doi:10.1016/j.atmosenv.2017.09.024, 2017.

Zheng, X. Y., Fu, Y. F., Yang, Y. J. and Liu, G. S.: Impact of atmospheric circulations on aerosol distributions in autumn over eastern China: Observational evidence, Atmos. Chem. Phys., 15(21), 12115–12138, doi:10.5194/acp-15-12115-2015, 2015.

Table 1. Over-limit ratio and concentration of MDA8 O_3 and PM2.5 calculated via stations × days in key urban clusters under four SWPs

Urban cluster	Month	Type1					Type2					Type3					Type4				
		Stas × days	MDA O_3		$PM_{2.5}$		Stas × days	MDA O_3		$PM_{2.5}$		Stas × days	MDA O_3		$PM_{2.5}$		Stas × days	$MDAO_3$		$PM_{2.5}$	
			OLR	Con	OLR	Con		OLR	Con	OLR	Con		OLR	Con	OLR	Con		OLR	Con	OLR	Con
BTH	6	6416	57.3%	172.5	16.7%	49.2	122	91.8%	209.6	3.3%	46.0	59	62.7%	176.0	32.2%	67.1	0	0	0	0	0
	7	1716	25.6%	134.2	21.2%	51.8	3681	54.2%	165.6	22.5%	56.9	1356	33.8%	141.8	12.9%	46.7	577	43.5%	153.7	8.8%	49.5
	8	1188	18.9%	118.5	6.9%	33.1	2805	35.3%	143.1	14.7%	44.0	1671	18.9%	121.2	10.1%	42.5	1268	31.9%	144.3	6.0%	39.7
	6~8	9320	46.6%	158.6	16.3%	47.6	365	54.2%	169.8	18.8%	51.2	3086	26.3%	131.3	11.7%	44.8	1845	35.5%	147.3	6.9%	42.8
YRD	6	19329	26.2%	127.2	4.4%	36.8	11098	14.3%	107.0	2.2%	44.5	181	12.7%	102.4	0.6%	32.0	0	0	0	0	0
	7	5207	24.5%	119.8	5.3%	38.6	8459	22.0%	120.1	0.6%	28.0	4135	14.5%	112.6	0.1%	24.0	1743	30.9%	139.5	0.3%	30.0
	8	3593	25.5%	127.6	0.3%	28.6	19922	18.3%	113.8	3.0%	33.3	4993	16.9%	116.7	0.0%	23.7	3817	14.7%	114.8	0.1%	25.1
	6~8	28129	25.8%	125.9	4.0%	36.1	13754	17.4%	112.5	1.7%	30.6	9309	15.8%	114.6	0.1%	24.0	5560	19.7%	122.5	0.1%	26.7
PRD	6	5327	5.2%	80.1	0	16.8	101	31.7%	146.9	0	24.9	48	0	77.6	0	13.2	0	0	0	0	0
	7	1431	20.3%	107.2	0.6%	25.3	3076	7.6%	81.8	0.1%	19.1	1079	13.3%	92.4	0	19.3	461	8.0%	82.1	0	17.9
	8	977	25.4%	122.5	1.1%	27.9	2316	20.6%	108.5	0.6%	28.0	1376	15.5%	103.4	0.3%	24.0	993	17.9%	111.4	0.1%	25.1
	6~8	7735	10.5%	90.5	0.2%	19.8	5493	13.5%	94.3	0.3%	23.0	2503	14.3%	98.2	0.2%	21.8	1454	14.8%	102.1	0.1%	22.8
GZP	6	1549	42.9%	147.6	0.4%	33.2	38	52.6%	165.3	0	30.4	19	26.3%	150.8	0	34.7	0	0	0	0	0
	7	1879	40.7%	145.0	1.9%	33.7	1168	47.4%	160.3	0	30.2	432	24.3%	133.3	1.2%	31.7	173	26.6%	144.1	0	26.4
	8	537	28.5%	134.0	1.6%	31.6	850	36.8%	146.3	1.6%	34.2	530	28.9%	143.1	1.9%	37.2	394	38.6%	154.9	1.3%	39.9
	6~8	368	15.2%	112.9	0.9%	32.4	2056	43.1%	154.6	2.1%	35.9	981	26.8%	138.9	1.5%	34.7	567	34.9%	151.6	0.9%	35.8
NEM	6	13126	17.9%	121.0	1.7%	26.4	243	64.2%	175.3	0.4%	31.1	120	13.3%	123.3	0.8%	37.6	0	0	0	0	0
	7	3422	8.9%	106.8	2.3%	25.2	7338	17.0%	120.7	1.3%	28.1	2722	5.7%	93.0	0.7%	20.8	1141	15.1%	122.4	0.2%	24.3
	8	2341	4.4%	92.6	1.0%	20.1	5520	6.3%	91.0	1.3%	21.0	3282	5.6%	98.3	0.9%	23.2	2507	7.8%	97.8	0.2%	19.5
	6~8	18889	14.6%	114.9	1.7%	25.4	13101	13.4%	109.2	1.3%	25.2	6124	5.8%	96.4	0.8%	22.4	3648	10.1%	105.5	0.2%	21.0

Notes: stas × days, stations × days; OLR, Over-limit ratio; Con, Concentration (μg m^{-3}).

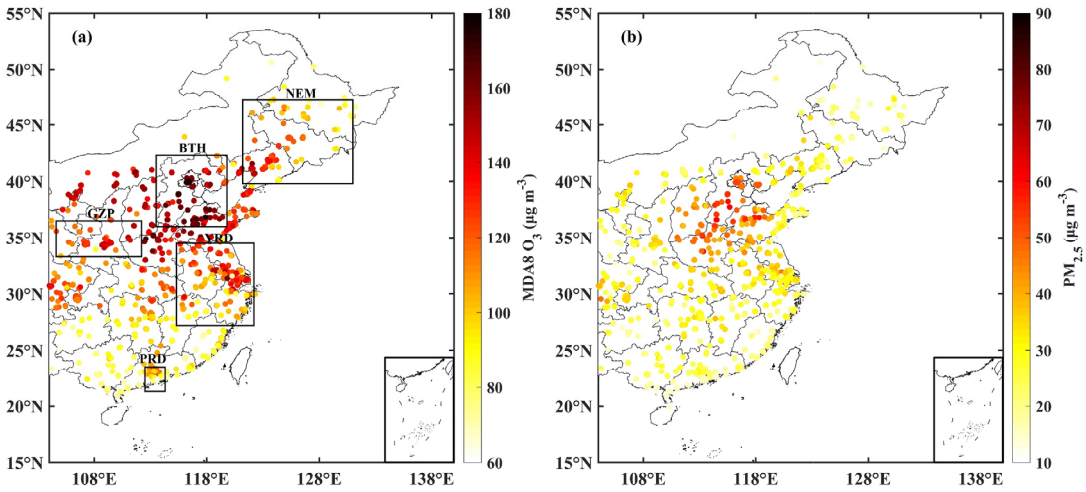

Fig. 1. Average concentration of MDA8 O_3 (a) and $PM_{2.5}$ (b) in eastern China during summers of 2015–2018. Stations and key urban clusters (black box) are shown in (a).

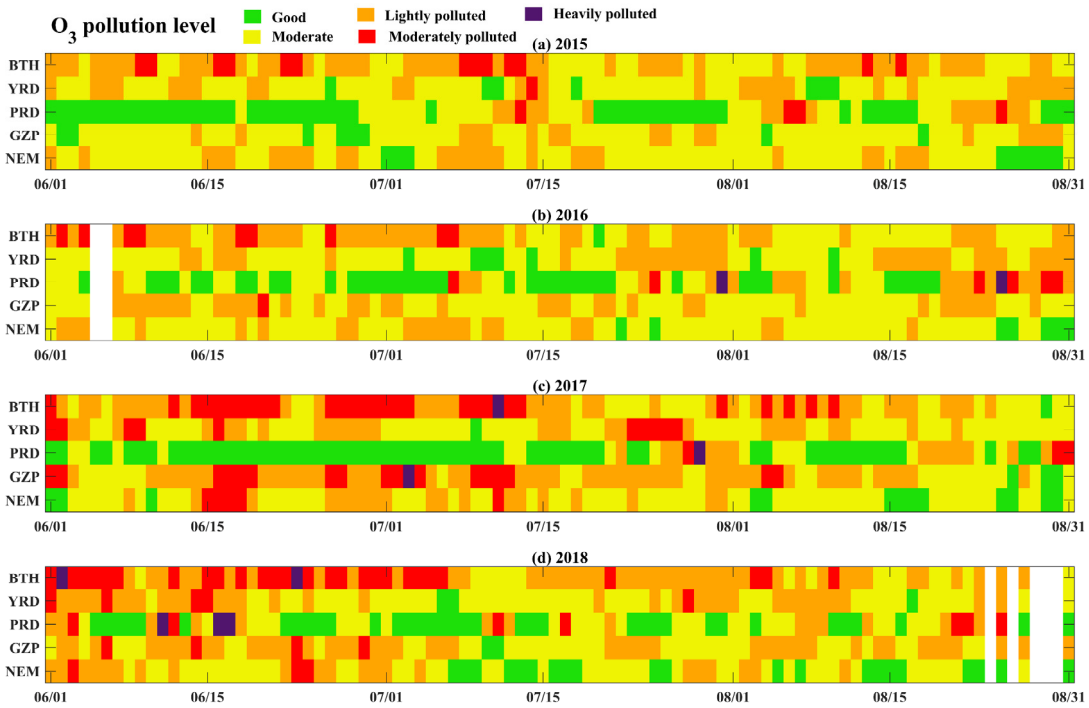

765

Fig. 2. Time series of MDA8 O_3 pollution levels in key urban clusters.

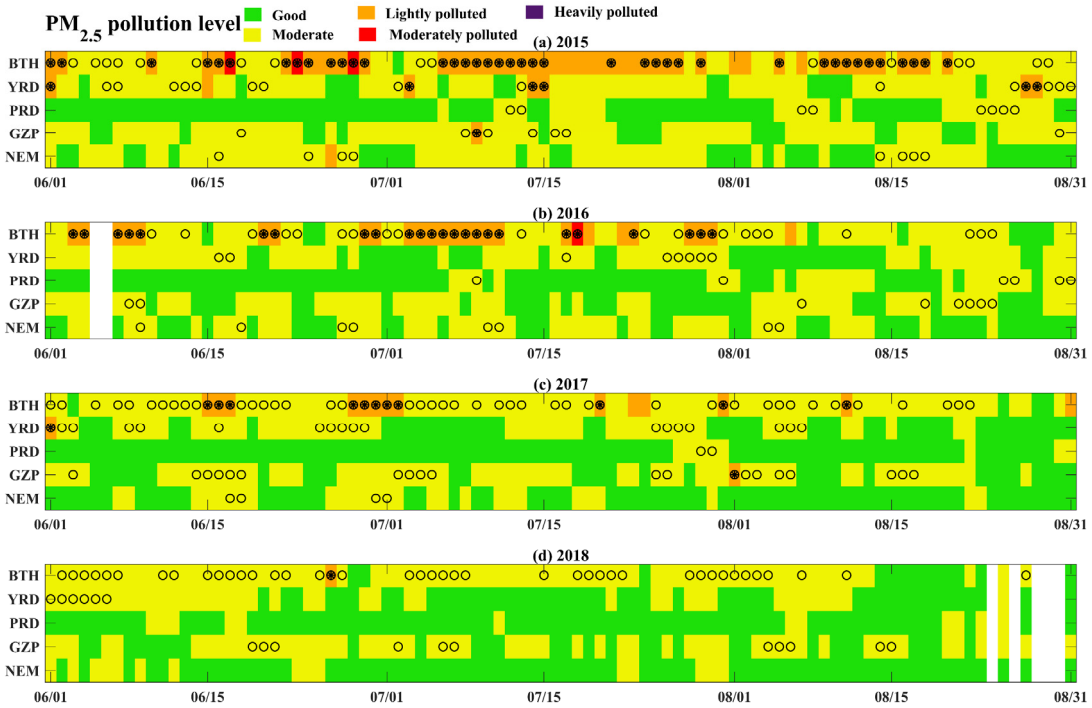

Fig.3. Time series of $PM_{2.5}$ pollution levels in key urban clusters. The black dots indicate the co-occurred events. The asterisks indicate the co-occurred events under Chinese standard (WHO interim target 1, IT-1), and the circles indicate the co-occurred events under WHO IT-2.

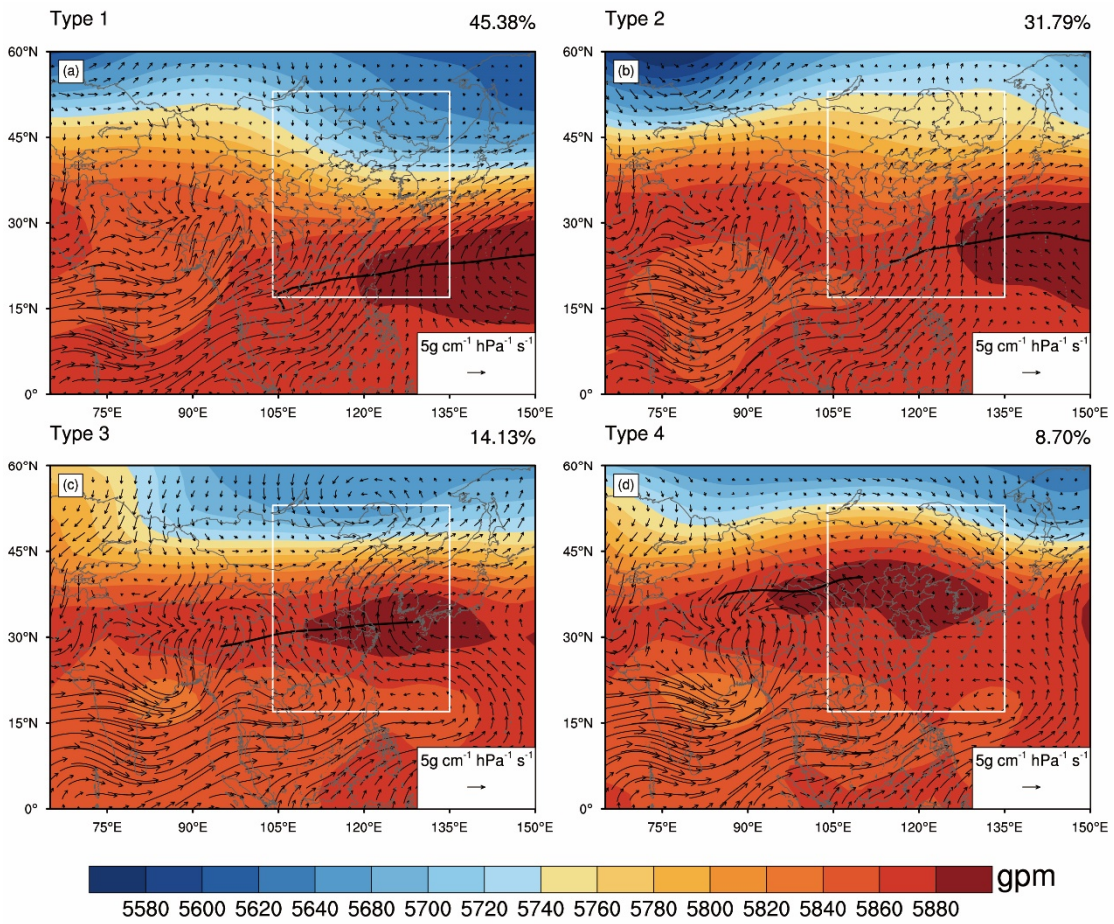

Fig. 4. 850-hPa 850 hPa water vapor flux ($WVF = V * q/g$, q is specific humidity, g is gravitational acceleration, V is horizonal wind; vectors; see scale arrow at the bottom right in units of 5 g cm^{-1}hPa^{-1}s^{-1}) and 500-hPa GH (contours; see scale bar at bottom in units of gpm) patterns based on objective classification (see text for details). White box area is for the area of eastern China, the number at the upper right corner of each panel indicates the frequency of the occurrence of each pattern type, and the black line of each panel presents the ridge axis of the WPSH.

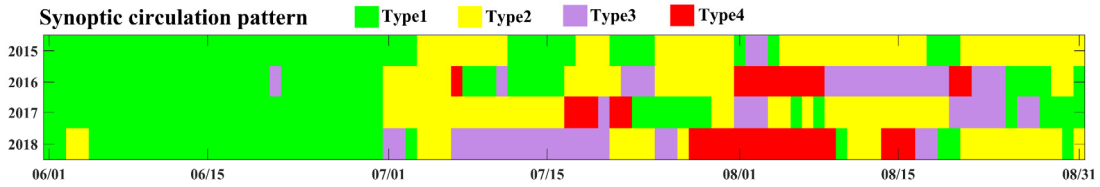

Fig. 5. Time series of synoptic circulation pattern.

785

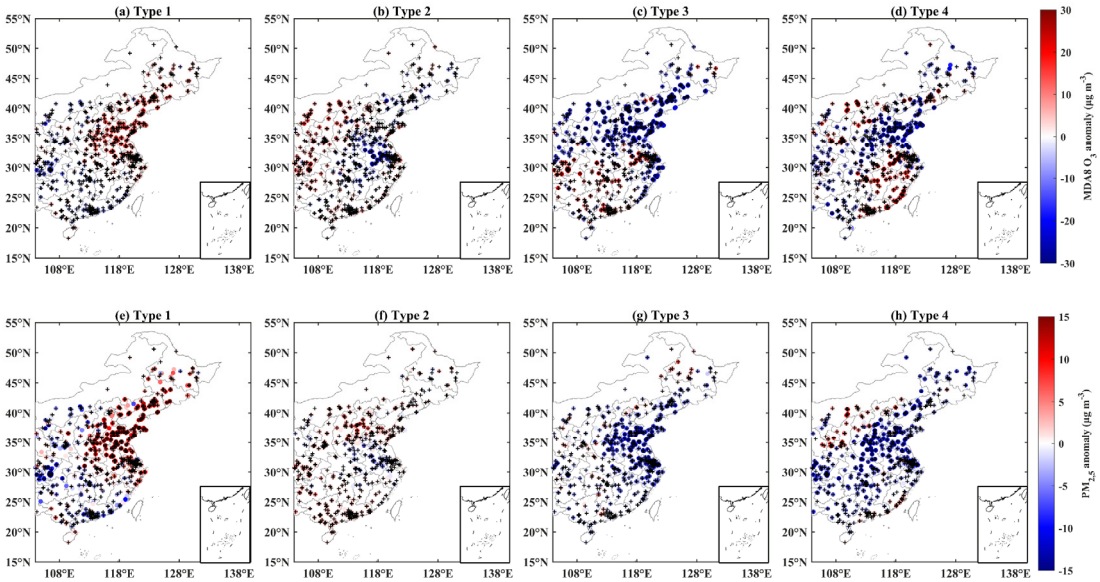

Fig. 6. The MDA8 O_3 (a-d) and $PM_{2.5}$ (e-h) anomaly under four SWPs, where the sites marked with a '+' indicates the Analysis of Variance passes the significance level of 0.05.

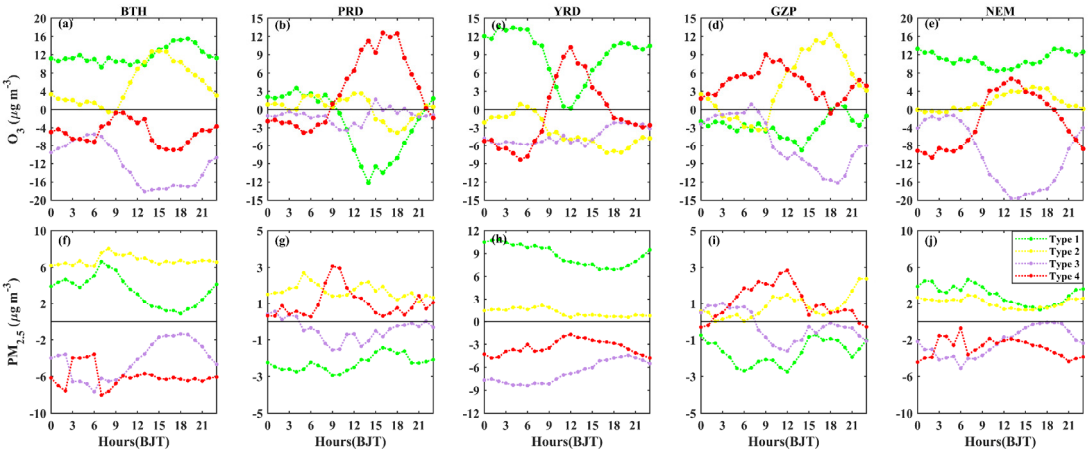

790

Fig. 7. Daily variation of O_3 and $PM_{2.5}$ anomalies under four SWPs in key urban clusters.

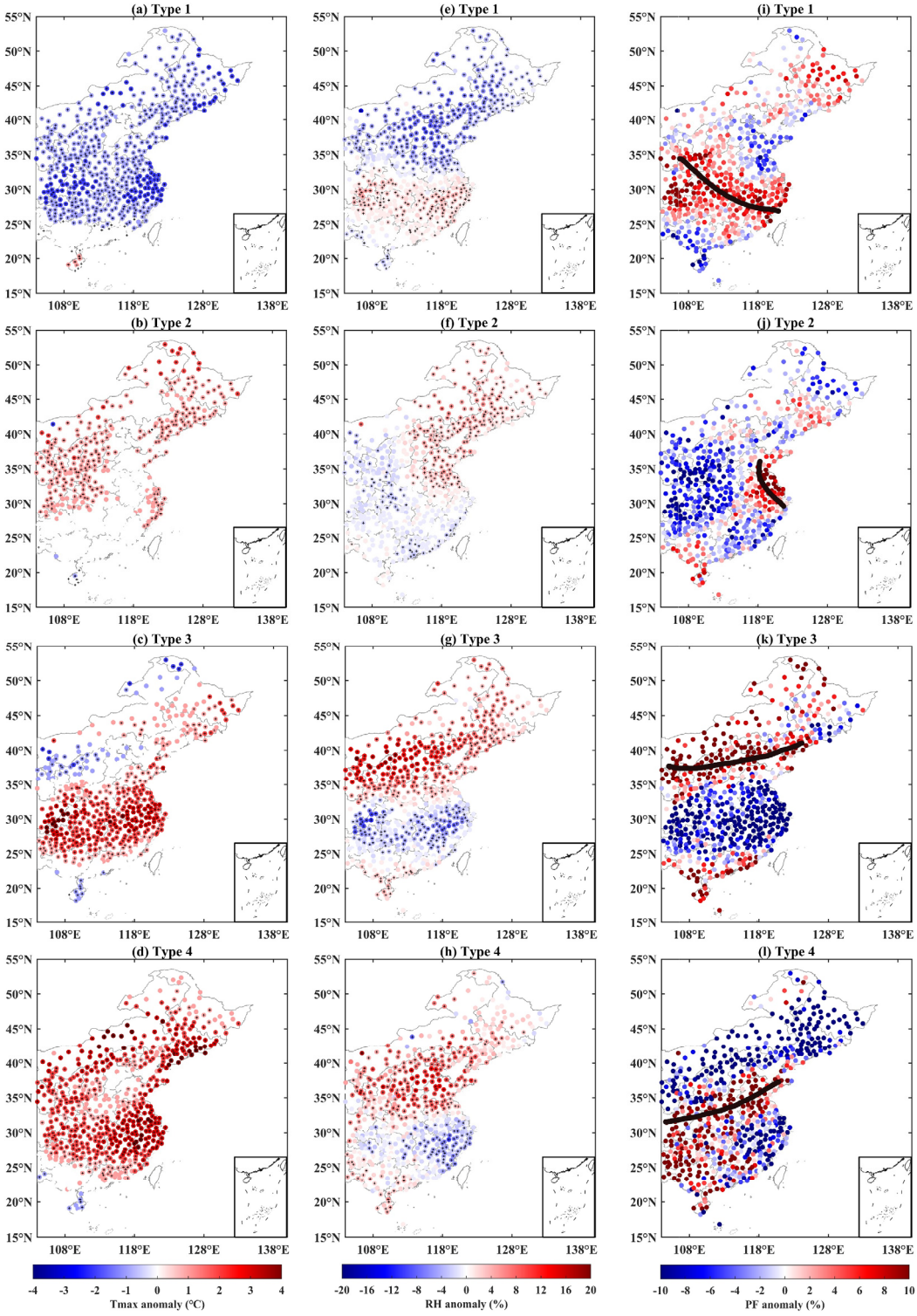

Fig. 8. Same as Fig. 6 but for Tmax (a–d), RH (e–h), and PF (i–l). The black solid line presents the rain belt of each SWP.

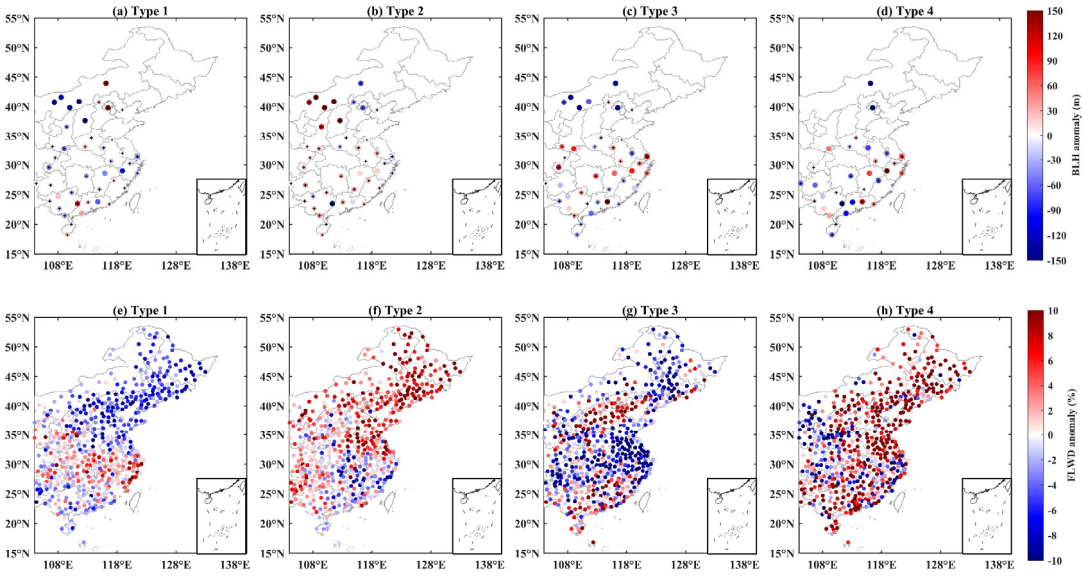

Fig. 9. Same as Fig. 6 but for BLH at 14:00 BJT (a–d) and FLWD (e–h).

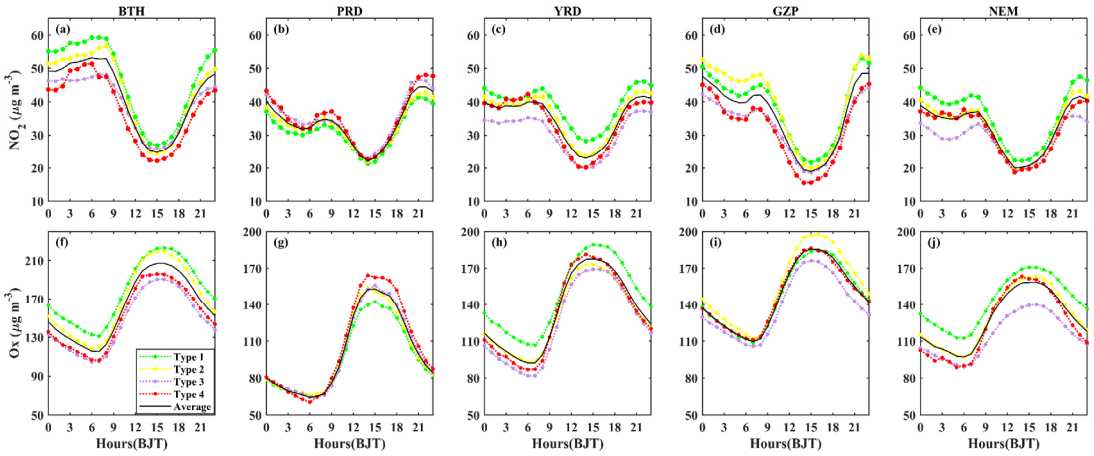

800 **Fig. 10. Daily variation of NO_2 (a-e) and Ox (f-j) under four SWPs in key urban clusters.**

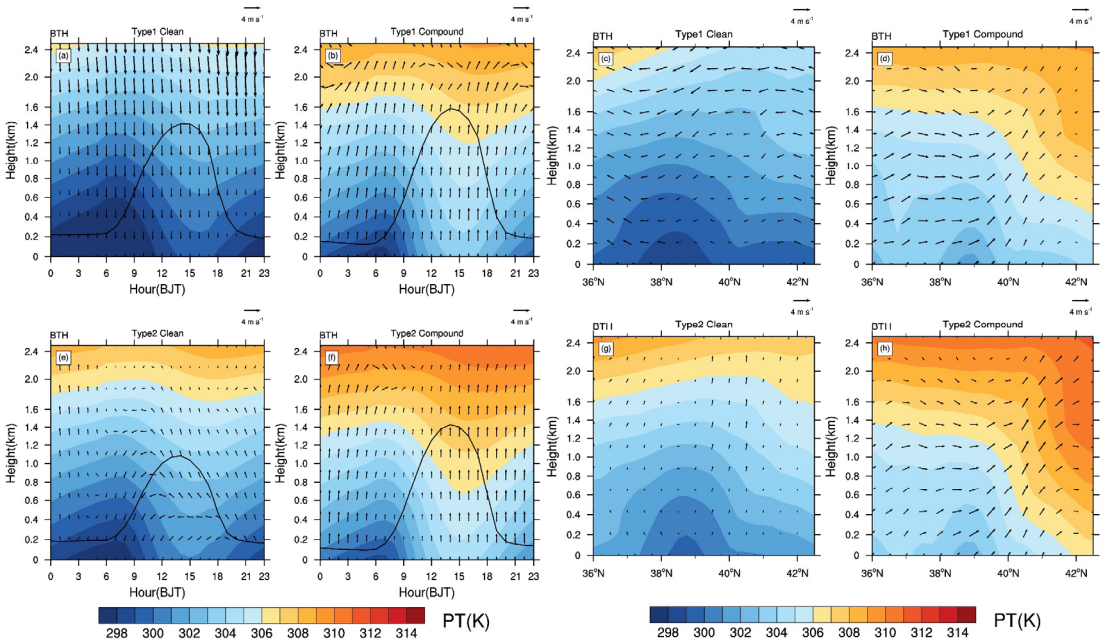

Fig. 11. The daily variation of horizonal wind, potential temperature (PT) and BLH of boundary layer in the BTH under clean and compound pollution period of Type 1 and Type 2 (a, b, e, f). The vertical cross-section of u-wind, w-wind and PT for the same situation of BTH (c, d, g, h). The w-wind is multiplied by 100 when used. The data has been derived from ERA5 reanalysis data.

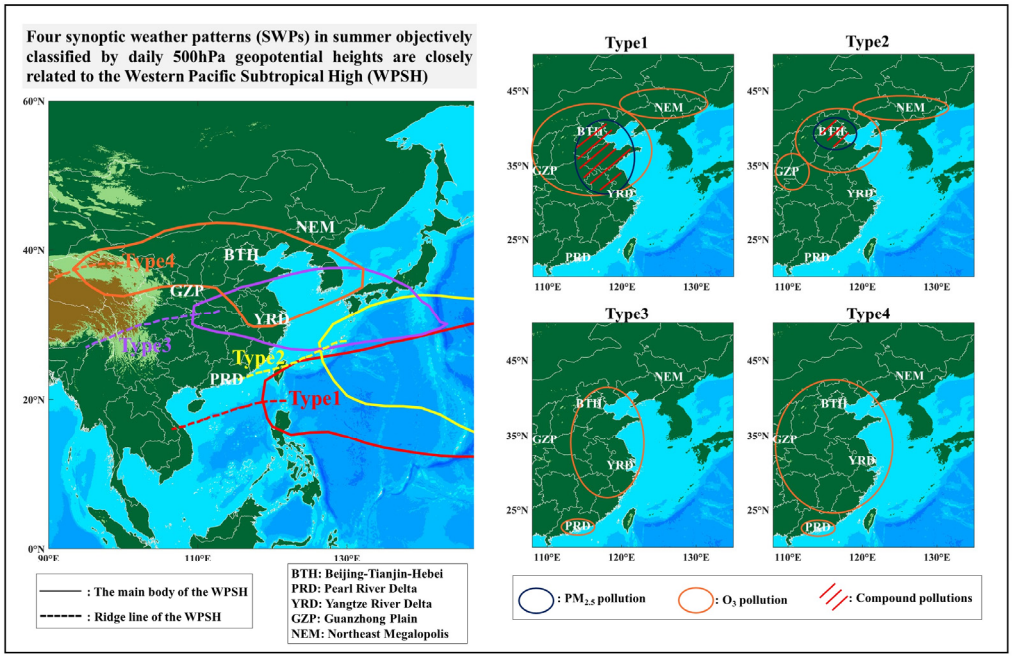

810

Fig. 12. Schematic diagrams describing the relationships between the WPSH, four SWPs and summertime O_3 and $PM_{2.5}$ pollution in various regions.